Optical Materials 124 (2022) 112050

Contents lists available at ScienceDirect

Optical Materials

journal homepage: www.elsevier.com/locate/optmat

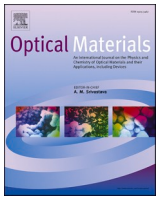

Growth of a novel $K_{0.4}Rb_{0.6}Pb_2Cl_5$ crystal and theoretical and experimental studies of its electronic and optical properties

O.Y. Khyzhun [a,*], Tuan V. Vu [b,c,**], A.A. Lavrentyev [d], B.V. Gabrelian [e], N.M. Denysyuk [a], L. I. Isaenko [f,g], M.S. Molokeev [h,i], A.A. Goloshumova [f,g], A.Y. Tarasova [f,g]

[a] Frantsevych Institute for Problems of Materials Science, National Academy of Sciences of Ukraine, 3 Krzhyzhanivsky Street, 03142, Kyiv, Ukraine
[b] Division of Computational Physics, Institute for Computational Science, Ton Duc Thang University, Ho Chi Minh City, Vietnam
[c] Faculty of Electrical & Electronics Engineering, Ton Duc Thang University, Ho Chi Minh City, Vietnam
[d] Department of Electrical Engineering and Electronics, Don State Technical University, 1 Gagarin Square, 344010, Rostov-on-Don, Russian Federation
[e] Department of Computational Technique and Automated System Software, Don State Technical University, 1 Gagarin Square, 344010, Rostov-on-Don, Russian Federation
[f] Laboratory of Functional Materials, Novosibirsk State University, 630090, Novosibirsk, Russian Federation
[g] Laboratory of Crystal Growth, V.S. Sobolev Institute of Geology and Mineralogy, SB RAS, 630090, Novosibirsk, Russian Federation
[h] Laboratory of Crystal Physics, Kirensky Institute of Physics, SB RAS, 660036, Krasnoyarsk, Russian Federation
[i] Research and Development Department, Kemerovo State University, Kemerovo, 650000, Russian Federation

ARTICLE INFO

Keywords:
Crystal growth
Ab initio calculations
X-ray photoelectron spectroscopy
Electronic structure
Optical properties

ABSTRACT

We report on successful growth by Bridgman method of an optical quality $K_{0.4}Rb_{0.6}Pb_2Cl_5$ crystal and determination of its crystal structure and electronic and optical properties. In particular, the present results indicate that the $K_{0.4}Rb_{0.6}Pb_2Cl_5$ crystal crystallizes in monoclinic space group $P2_1/c$, with the unit-cell parameters as follows: a = 8.9484(2) Å, b = 7.9802(2) Å, c = 12.5359 Å, and β = 90.1220(10)°. For the $K_{0.4}Rb_{0.6}Pb_2Cl_5$ crystal, we use X-ray photoelectron spectroscopy (XPS) to measure binding energies of the core-level electrons for constituting atoms and to reveal the energy distribution of the valence electronic states. Our XPS measurements indicate very low hygroscopicity of the $K_{0.4}Rb_{0.6}Pb_2Cl_5$ crystal surface and partial alteration from Pb^{2+} ions to Pb^0 when using bombardment with 3 kV Ar^+ ions. To find peculiarities of filling the valence band and the conduction band of the $K_{0.4}Rb_{0.6}Pb_2Cl_5$ crystal by partial densities of electronic states associated with the composing atoms, we apply different approaches for exchange-correlation potential using model $K_{0.5}Rb_{0.5}Pb_2Cl_5$ solid solution. We have found that the finest agreement of the experimental and theoretical data is derived when in the calculating procedure we use Tran-Blaha modified Becke-Johnson (TB-mBJ) potential involving spin-orbit coupling and the Hubbard parameter U (TB-mBJ + U + SOC approach). The present theoretical TB-mBJ + U + SOC results predict that $K_{0.5}Rb_{0.5}Pb_2Cl_5$ is a non-direct material with energy band gap of 4.167 eV. The optical properties of $K_{0.5}Rb_{0.5}Pb_2Cl_5$ are elucidated theoretically in detail based on first-principles calculations within the TB-mBJ + U + SOC model.

1. Introduction

In recent years, a lot of attempts of scientists and engineers have been made for developing non-linear crystals, promising low-phonon-frequency hosts for inserting diverse rare-earth (RE) ions, with the aim of their further use in the compact solid-state laser systems applied for generation at ambient conditions in a rather wide spectral range spreading from mid-infrared (mid-IR) up to vacuum ultraviolet [1]. Such solid-state laser systems are found to be very promising for application in different important areas, e.g. thermal imaging, clinic diagnostics, medical surgery, free space communication, probing bio-chemical agents, precise detection of drugs, fingerprint sensors, etc. [2–8]. Among prospective low-phonon-frequency hosts, series of alkali- and lead-bearing halide crystals describing by a general formula APb_2X_5 (where A stands for K and Rb; while X designates either Cl or Br) attract tremendous attention [1]. Such APb_2X_5 crystals are found to be very

* Corresponding author.
** Corresponding author. Division of Computational Physics, Institute for Computational Science, Ton Duc Thang University, Ho Chi Minh City, Viet Nam.
E-mail addresses: khyzhun@ipms.kiev.ua (O.Y. Khyzhun), vuvantuan@tdtu.edu.vn (T.V. Vu).

https://doi.org/10.1016/j.optmat.2022.112050
Received 26 December 2021; Received in revised form 20 January 2022; Accepted 26 January 2022
Available online 2 February 2022

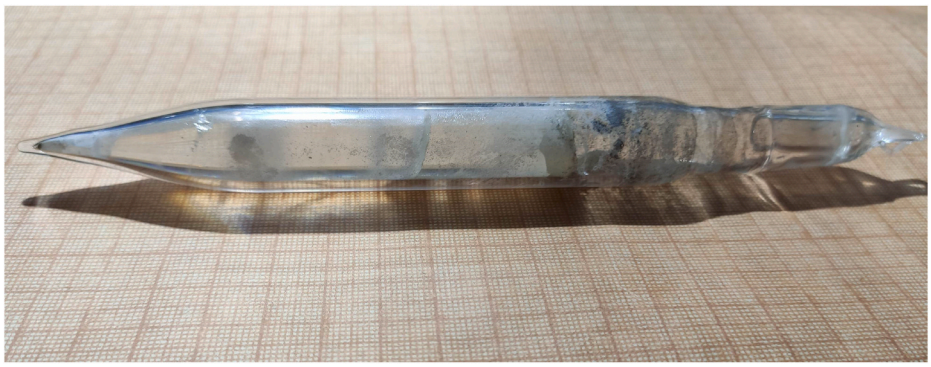

Fig. 1. A photo of the $K_{0.4}Rb_{0.6}Pb_2Cl_5$ single crystal applied in the present experiments.

prospective hosts for embedding a number of RE ions, particularly Nd^{3+}, Dy^{3+}, Pr^{3+}, Er^{3+}, Ho^{3+}, Tb^{3+}, and Tm^{3+} [9–15] as well as U^{3+} [16], Yb^{3+} [17], and Mn^{2+} [18]. The APb_2X_5 crystals, depending on the kind of the embedding ions, reveal operating abilities in a broader spectral area, with increasing emission properties and smaller luminescence decay ratios [19].

Potassium and rubidium lead-containing chlorides, KPb_2Cl_5 and $RbPb_2Cl_5$, are of particular interest. These ternary compounds crystallize in a monoclinic structure, space group $P2_1/c$, with the following unit-cell parameters: a = 8.831 Å, b = 7.886 Å, c = 12.43 Å, and β = 90.05° for KPb_2Cl_5 and a = 8.959 Å, b = 7.973 Å, c = 12.493 Å, and β = 90.12° for $RbPb_2Cl_5$ [20]. These crystals are biaxial and transparent in a broad spectral interval ranging from 0.3 till 20 μm [20]. The KPb_2Cl_5 and $RbPb_2Cl_5$ crystals reveal almost the same energy band gaps, 4.79 and 4.83 eV, respectively, as measurements of the reflection spectra at 8 K indicate [21]. With respect to a solid state KPb_2Cl_5–$RbPb_2Cl_5$ solution, the data are scarce.

Since the knowledge concerning the electronic structure of a solid and peculiarities of the formation of chemical bonds in it plays a rather notable role in clarifying the physical/chemical properties and predicting possible ways for their modification to gain desirable technological parameters [22], the electronic properties of KPb_2Cl_5 were studied in Refs. [21,23] employing X-ray photoelectron spectroscopy (XPS), while ab initio band-structure calculations of this ternary chloride were performed in Ref. [23]. The XPS measurements [21,23] indicated minor hygroscopicity of KPb_2Cl_5 crystal and partial minor alterations of Pb^{2+} ions to Pb^0 under bombardment of its surface with 3 keV Ar^+ ions. The band-structure calculations [23] performed within density functional theory (DFT) revealed strong covalent nature of the Pb–Cl bonds in KPb_2Cl_5 and the domination of Cl p and Pb s states in the upper part and near the bottom of the valence band, respectively. The conduction band bottom of KPb_2Cl_5 is formed substantially due to the input of unoccupied p states originated from lead and chlorine atoms [23].

The studies of physicochemical properties of $K_xRb_{1-x}Pb_2Cl_5$ solid solution are insufficient. Comparatively recently Lichkova et al. [24] reported on successful synthesis of double salt $K_{0.5}Rb_{0.5}Pb_2Cl_5$. The authors [24] determined that the double salt $K_{0.5}Rb_{0.5}Pb_2Cl_5$ is isostructural to KPb_2Cl_5 with somewhat smaller unit-cell parameters. However, the lattice parameters of the double salt $K_{0.5}Rb_{0.5}Pb_2Cl_5$ were not reported by Lichkova et al. [24]. To the best our knowledge, there are no data on changes in the electronic band-structure and optical properties when substituting potassium in KPb_2Cl_5 by rubidium when forming $K_xRb_{1-x}Pb_2Cl_5$ solid solution. To overcome this lack, here we report on successful growth of $K_{0.4}Rb_{0.6}Pb_2Cl_5$ crystal by Bridgman method and its studies with the XPS technique to estimate binding energies (BEs) of the constituting atoms and energy distribution of the valence electronic states. We have also explored the impact of middle-energy Ar^+ ion-treatment on the chemical stability of the $K_{0.4}Rb_{0.6}Pb_2Cl_5$ crystal surface. To examine the data of our XPS measurements, we present also details of DFT calculations regarding total and projected densities of states (DOS) of representative $K_{0.5}Rb_{0.5}Pb_2Cl_5$ solid solution and explore thoroughly its optical constants. The present experimental and theoretical data for $K_xRb_{1-x}Pb_2Cl_5$ solid solutions are compared with similar XPS measurements and DFT calculations made recently for ternary KPb_2Cl_5 chloride [23].

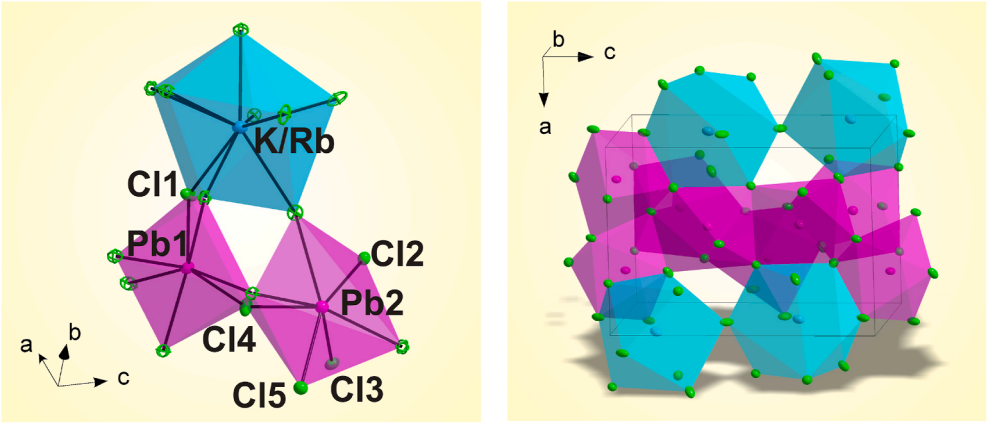

(a) (b)

Fig. 2. (a) Asymmetric part of the unit cell of the $K_{0.4}Rb_{0.6}Pb_2Cl_5$ compound (the non-equivalent atoms are labeled) and (b) arrangement of the atoms in this compound (Note: in the latter case, the unit cell is outlined and the ellipsoids are drawn at the 50% probability level).

Table 1
Crystal structure parameters of the $K_{0.4}Rb_{0.6}Pb_2Cl_5$ compound under study.

Single crystal	$K_{0.4}Rb_{0.6}Pb_2Cl_5$
Moiety formula	$Cl_{10}K_{0.77}Pb_4Rb_{1.23}$
Dimension (mm)	0.3 × 0.2 × 0.1
Color	colorless
Molecular weight	1318.26
Temperature (K)	296
Space group, *Z*	$P2_1/c$, 2
a (Å)	8.9484 (2)
b (Å)	7.9802 (2)
c (Å)	12.5359 (3)
α (°)	90
β (°)	90.1220 (10)
γ (°)	90
V (Å^3)	895.19 (4)
ρ_{calc} (g/cm^3)	4.890
μ (mm^{-1})	42.435
Reflections measured	10,173
Reflections independent	3018
Reflections with $F > 4\sigma(F)$	2698
$2\theta_{max}$ (°)	72.62
h, *k*, *l* - limits	$-14 \le h \le 14$; $-13 \le k \le 13$; $-20 \le l \le 20$
R_{int}	0.0583
The weighed refinement of F^2	$w = 1/[\sigma^2(F_o^2)+(0.1534P)^2]$, $P = (F_o^2+2F_c^2)/3$
Number of refinement parameters	75
*R*1 [$F_o > 4\sigma(F_o)$]	0.0726
w*R*2	0.01996
Goof	1.083
$\Delta\rho_{max}$ (e/Å^3)	4.90
$\Delta\rho_{min}$ (e/Å^3)	−5.08
$(\Delta/\sigma)_{max}$	0.000

2. Experimental

2.1. Crystal growth

The synthesis of $K_{0.4}Rb_{0.6}Pb_2Cl_5$ crystal was made employing high purity chloride salts. The initial high purity (99.999%) chemical components, $PbCl_5$, KCl and RbCl, were further purified applying the iterating directed crystallization through removing initial dirty parts. The $K_{0.4}Rb_{0.6}Pb_2Cl_5$ single crystal was grown using Bridgman method in a soldered ampoule with halide-containing atmosphere. Linear temperature gradient of a furnace zone corresponding to growth process was set to be equal to ~20 °C/cm, and the moving ampoule rate into the cold furnace part was chosen to be in the range from 2 to 4 mm/day. We established that these operation conditions are sufficient for obtaining optical quality $K_{0.4}Rb_{0.6}Pb_2Cl_5$ single crystals with dimensions of ~18 mm in diameter and 35 mm long. A photo of the optical quality $K_{0.4}Rb_{0.6}Pb_2Cl_5$ crystal applied in the present experimental studies is shown in Fig. 1.

2.2. Single crystal X-ray diffraction (XRD) analysis

The single crystal X-ray data were collected for the $K_{0.4}Rb_{0.6}Pb_2Cl_5$ crystal at 296 K using a SMART APEX II single crystal diffractometer (Bruker AXS, analytical equipment of Krasnoyarsk Center for the collective use of SB RAS) supplied with a CCD-detector, graphite monochromator and using Mo Kα radiation. The orientation matrix and cell parameters were estimated and the latter were refined using the total set of 10,173 reflections. The present single crystal XRD findings indicate that the $K_{0.4}Rb_{0.6}Pb_2Cl_5$ crystal unit cell corresponds to monoclinic symmetry. Space group $P2_1/c$ was established based on statistical analysis of intensities of all the reflections. The absorption corrections were applied using the SADABS program [25]. The crystal structure was determined by the direct methods applying the package SHELXS and refined in the anisotropic approach for all atoms using the SHELXL program [26]. The structure test for the presence of skipped symmetry elements and possible voids was performed employing the program PLATON [27]. The DIAMOND program [28] was applied for the crystal structure plotting (Fig. 2). The single crystal X-ray data for $K_{0.4}Rb_{0.6}Pb_2Cl_5$ are listed in Table 1.

2.3. X-ray photoelectron spectroscopy measurements

The technical details for XPS experiments of the $K_{0.4}Rb_{0.6}Pb_2Cl_5$ crystal presented here are completely the same as we reported earlier for related ternary KPb_2Cl_5 chloride [23]. Briefly, the UHV Analysis System designed and constructed by SPECS Surface Nano Analysis Company (Berlin, Germany) was used for such a goal. The XPS spectra were originated by employing an X-ray Mg Kα source and were acquired at constant pass energy of 30 eV. The technique of surface preparation for XPS measurements is similar to that reported elsewhere [29].

3. Computational method

To verify data of the present experimental XPS measurements of the $K_{0.4}Rb_{0.6}Pb_2Cl_5$ crystal, we have made also DFT calculations of its electronic structure. For such a purpose, we employ possibilities of the full potential augmented plane wave + local-orbital (FP-APW-LO) method as realized within the WIEN2k package [30]. Since the WIEN2k package does not allow calculating the electronic structure for compounds possessing different atoms occupying the same crystal positions, we have used the model employed previously for DFT calculations of the related $K_{0.5}Rb_{0.5}Pb_2Br_5$ bromide [31]. In such a case, the optimized 1 × 1 × 2 supercell of the ternary KPb_2Cl_5 chloride is used. In this model, one potassium atom of KPb_2Cl_5 is replaced by one rubidium atom leading to the $K_{0.5}Rb_{0.5}Pb_2Cl_5$ composition. This composition is somewhat different from experimental one, $K_{0.4}Rb_{0.6}Pb_2Cl_5$. However, our attempts to construct special supercells for the $K_{0.4}Rb_{0.6}Pb_2Cl_5$ composition were insufficient, unfortunately. Previous DFT calculations of $K_{0.5}Rb_{0.5}Pb_2Br_5$ and KPb_2Br_5 bromides indicate [31,32] that the main contributions in their valence band and conduction band regions come from electronic states related to lead and bromine atoms, while those associated with potassium/rubidium are quite minor. We believe that this is characteristic for the related chlorides, too.

In our DFT calculations, following the muffin-tin (MT) approach, we use the unit cell of the $K_{0.4}Rb_{0.6}Pb_2Cl_5$ crystal (Table 1) that was divided into atomic spheres and interstitial regions. The MT radii of potassium, rubidium, lead, and chlorine were used to be equal to 2.5, 2.5, 2.5 and 2.4 a.u., respectively (note that 1 a.u. = 0.529177 Å). In the calculations, we expand wavefunctions till the maximum angular momentum $l_{max} = 10$, whereas the charge density we expand employing Fourier series with $G_{max} = 12$ a.u.$^{-1}$. To explore the best agreement of the present theoretical DOS curves with the experimental XPS spectrum, we treat for exchange-correlation (XC) potential the commonly used generalized gradient approximation (GGA) as defined by Perdew, Burke, and Ernzerhof (GGA-PBE) [33] and Becke-Johnson functional modified in the form of Tran and Blaha (TB-mBJ) [34,35]. In addition, we verify in our DFT calculations made within the GGA-PBE and TB-mBJ approaches the effects of Coulomb repulsion (the so-called Hubbard parameter U) [36,37] and spin-orbital coupling (SOC) [38]. We use a 1000 *k*-point mesh in the Brillouin zone (BZ), while the parameter, $R_{min}^{MT}K_{max}$ where R_{min}^{MT} denotes the minimum MT sphere radius and k_{max} designates the value of the biggest *k* vector in the plane wave extension, is equal to 7.0. When using these parameters, differences in out-put charge densities $q = \int|P_n - P_{n-1}|dr$ were found to be smaller than 10^{-4} Ry.

4. Results and discussion

4.1. Crystal structure of $K_{0.4}Rb_{0.6}Pb_2Cl_5$ as determined by XRD

The present XRD data listed in Table 1 indicate that the

Table 2
Fractional atomic coordinates and isotropic or equivalent isotropic displacement parameters (Å^2) of the $K_{0.4}Rb_{0.6}Pb_2Cl_5$ crystal under study.

Atom	*x*	*y*	*z*	U_{iso}*/U_{eq}	*Occupancy*
Pb1	0.75309 (4)	0.56243 (5)	0.00620 (3)	0.01960 (18)	1
Pb2	0.50625 (6)	0.50631 (6)	0.32619 (4)	0.02295 (19)	1
Rb	0.98989 (19)	1.0567 (2)	0.16785 (14)	0.0278 (5)	0.609 (15)
K	0.98989 (19)	1.0567 (2)	0.16785 (14)	0.0278 (5)	0.391 (15)
Cl1	1.0400 (3)	0.6800 (4)	0.0771 (3)	0.0283 (6)	1
Cl2	0.7174 (3)	0.5420 (4)	0.5016 (2)	0.0212 (4)	1
Cl3	0.5419 (3)	0.1656 (3)	0.4027 (2)	0.0207 (4)	1
Cl4	0.7258 (4)	0.3467 (4)	0.1889 (2)	0.0285 (6)	1
Cl5	0.2681 (3)	0.3127 (3)	0.2202 (2)	0.0237 (5)	1

Table 3
The main bond lengths (Å) of the $K_{0.4}Rb_{0.6}Pb_2Cl_5$ crystal.

Pb1–Cl1	2.872 (3)	Rb–Cl1	3.246 (3)
Pb1–Cl1^{i}	2.876 (3)	Rb–Cl5^{ix}	3.286 (3)
Pb1–Cl4	2.876 (3)	Rb–Cl2^{x}	3.299 (3)
Pb1–Cl3^{ii}	2.925 (2)	Rb–Cl4^{xi}	3.318 (3)
Pb1–Cl3^{iii}	2.994 (2)	Rb–Cl5^{iii}	3.332 (3)
Pb1–Cl5^{iv}	3.014 (3)	Rb–Cl1^{xii}	3.357 (4)
Pb2–Cl3	2.900 (2)	Rb–Cl2^{xii}	3.378 (3)
Pb2–Cl4	2.909 (3)	Rb–Cl4^{xii}	3.534 (4)
Pb2–Cl2	2.911 (3)	Rb–Cl1^{v}	3.730 (4)
Pb2–Cl5	2.946 (3)		
Pb2–Cl2^{vi}	2.972 (3)		

Note: Symmetry codes are following: (i) -*x*+2, -*y*+1, -*z*; (ii) *x*, -*y*+1/2, *z*-1/2; (iii) -*x*+1, *y*+1/2, -*z*+1/2; (iv) -*x*+1, -*y*+1, -*z*; (v) -*x*+2, -*y*+2, -*z*; (vi) -*x*+1, -*y*+1, -*z*+1; (vii) -*x*+1, *y*-1/2, -*z*+1/2; (viii) -*x*+2, *y*-1/2, -*z*+1/2; (ix) *x*+1, *y*+1, *z*; (x) *x*, -*y*+3/2, *z*-1/2; (xi) *x*, *y*+1, *z*; (xii) -*x*+2, *y*+1/2, -*z*+1/2.

$K_{0.4}Rb_{0.6}Pb_2Cl_5$ crystal possesses a monoclinic structure type, space group $P2_1/c$, with the unit-cell parameters as follows: a = 8.9484(2) Å, b = 7.9802(2) Å, c = 12.5359 Å, and β = 90.1220(10)°. The crystallographic data deposited in Cambridge Crystallographic Data Centre (CSD # 2126666). These data can be downloaded from the site (www.ccdc.cam.ac.uk/data_request/cif). Comparison of these data with those reported for KPb_2Cl_5 (a = 8.831 Å, b = 7.886 Å, c = 12.43 Å, and β = 90.05° [20]) indicates that the unit-cell parameters increase when going from KPb_2Cl_5 to $K_{0.4}Rb_{0.6}Pb_2Cl_5$. The coordinates of atoms in the $K_{0.4}Rb_{0.6}Pb_2Cl_5$ crystal are listed in Table 2, while Table 3 presents data of determination of main bond lengths. The asymmetric part of the unit cell involves two Pb^{2+} ions, one site is occupied by Rb^+/K^+ ions, and five Cl^- ions. Each Pb^{2+} ion is coordinated by seven Cl^- ions forming monocapped trigonal $PbCl_7$ prisms which are connected with each other by edges (Fig. 2a). The Rb^+/K^+ ion is surrounded by nine Cl^- ions forming a $(Rb,K)Cl_9$ polyhedron which is connected to $PbCl_7$ prisms through nodes, forming a 3D net (Fig. 2b). The refinement of Rb:K ratio reveals the chemical formula $K_{0.39(2)}Rb_{0.61(2)}Pb_2Cl_5$ which is close to the suggested one, $K_{0.4}Rb_{0.6}Pb_2Cl_5$.

It is worth noting that, a Pb^{2+} ion is known to possess a lone pair of electrons (the so-called '$6s^2$' lone pair of electrons) revealing substantial stereochemical activity in solids [39,40] and generally causing significant amount of partial local disorder at special crystal local sites in such a case [41]. The effect of stereochemical activity of the '$6s^2$' lone pair of electrons accompanies by the formation of lead-centered non-centrosymmetric polyhedra originated as a result of John-Teller distortion [42]. Therefore, some lead bearing halides and chalcogenides possess a well-pronounced noncentrosymmetric crystal structure and are considered novel materials for non-linear optics [43–45]. In spite of the fact that such materials contain lead, a well-recognized hazardous chemical element, they are found to be rather stable as a number of experimental findings indicate [46,47].

4.2. XPS measurements of the $K_{0.4}Rb_{0.6}Pb_2Cl_5$ crystal

Fig. 3 presents data of the present measurements of survey XPS spectra of $K_{0.4}Rb_{0.6}Pb_2Cl_5$ crystal surfaces, both as-grown and bombarded with 3000 eV Ar^+ ions. From this figure, one can see that all XPS spectral features are well assigned to the atoms consisting the crystal under consideration. Some small signals ascribed to the C(O) 1s lines visible on the survey XPS spectrum of the as-derived $K_{0.4}Rb_{0.6}Pb_2Cl_5$ crystal surface are explained by hydrocarbon- and oxygen-containing

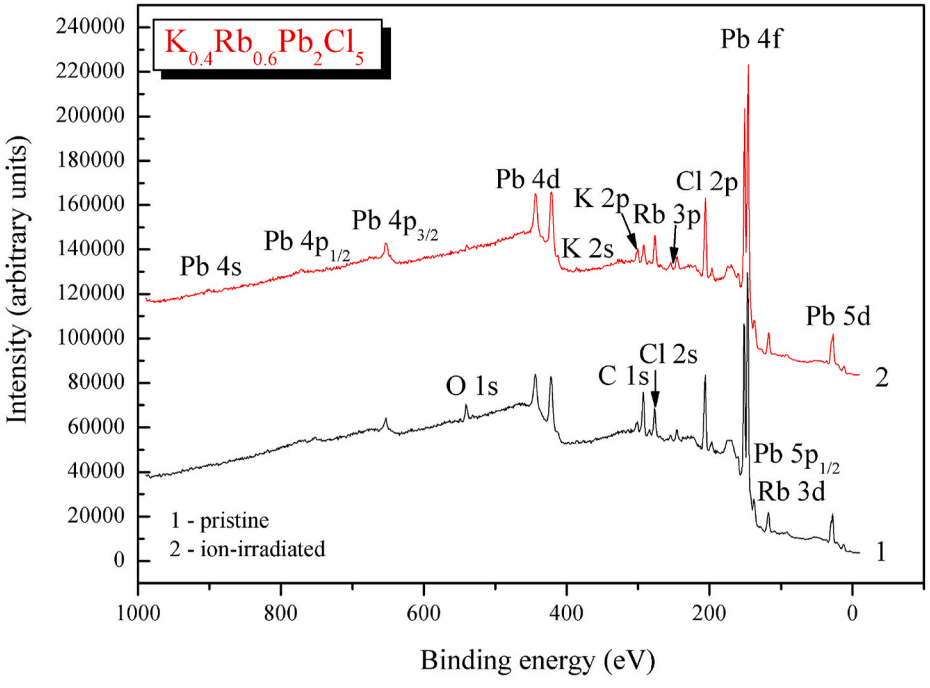

Fig. 3. Survey XPS spectra of the $K_{0.4}Rb_{0.6}Pb_2Cl_5$ crystal: (1) initial surface and (b) Ar^+-ion-irradiated surface.

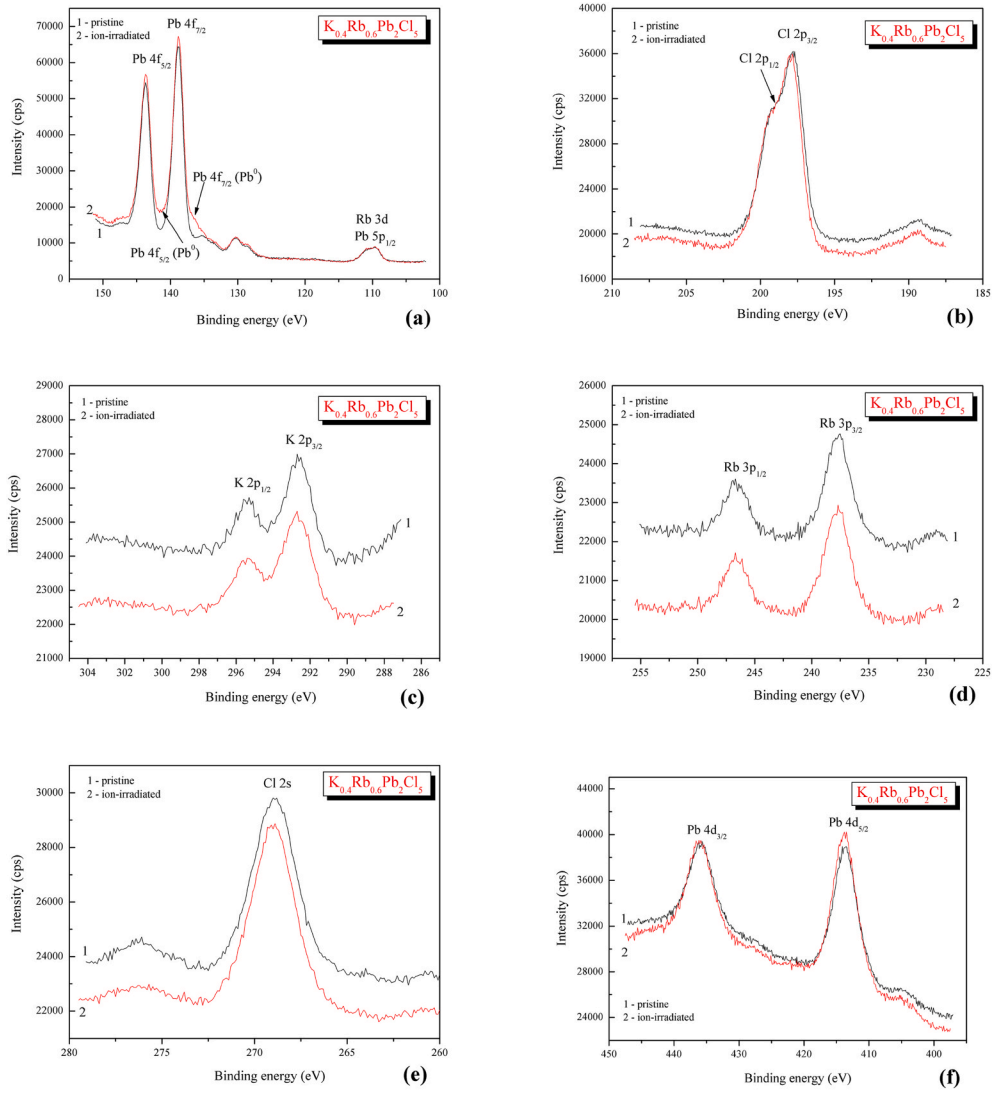

Fig. 4. Core-level XPS (a) Pb 4f, (b) Cl 2p, (c) K 2p, (d) Rb 3p, (e) Cl 2s, and (f) Pb 4d spectra of the $K_{0.4}Rb_{0.6}Pb_2Cl_5$ crystal: (1) initial surface and (b) Ar^+-ion-irradiated surface.

species caused by crystal exposure to laboratory air for a couple of days prior the XPS measurements began. However, the relative intensities of the C(O) 1s lines are decreased abruptly after about 5 min bombardment of the surface with 3000 eV Ar^+ ions (full ions flux was measured to be about 5.4×10^{16} ions·cm^{-2}) indicating rather small degree of hygroscopicity of the $K_{0.4}Rb_{0.6}Pb_2Cl_5$ crystal surface. This peculiarity of the crystal under consideration looks to be similar to those proved previously to be specific of the related chloride KPb_2Cl_5 [23] and bromides K(Rb)Pb_2Br_5 [29].

The most demonstrative core-level XPS spectra of potassium, rubidium, lead and chlorine atoms composing the $K_{0.4}Rb_{0.6}Pb_2Cl_5$ crystal are presented in Fig. 4, while binding energy values for core-level electrons associated with those atoms are gathered in Table 4. The XPS data presented in Fig. 4 demonstrate that we do not see any substantial alterations of the spectra peculiarities when irradiating the $K_{0.4}Rb_{0.6}Pb_2Cl_5$ crystal surface with 3000 eV Ar^+ ions. Nevertheless, such a surface treatment causes the appearance of spectral features associated with lead (see, e.g., the XPS core-level Pb 4f (Fig. 4a) and Pb 5d (Fig. 5) spectra) in the charge state Pb^0. The latter species reach about 6.8% as our estimations using measurements of the Pb 4f spectra of the $K_{0.4}Rb_{0.6}Pb_2Cl_5$ crystal indicate. These XPS results feature subtle conversion of the Pb^{2+} ions to Pb^0 when irradiating the crystal surface under study with middle-energy Ar^+ ions. Similar transformation of Pb^{2+} ions to Pb^0 amounting to 7.5% at the same full ions flux was detected previously when studying the relative ternary KPb_2Cl_5 chloride [23]. As a result, we detect minor shifts of the core-level XPS spectra related to lead atoms toward the side of smaller BEs, whereas those associated with chlorine atoms yield slight shifts toward bigger BEs (Table 4). At the above surface treatment of the $K_{0.4}Rb_{0.6}Pb_2Cl_5$ crystal we do not see changes of the BEs for the K 2p and Rb 3p core-level electrons (Fig. 4, Table 4) as well as energy allocation of the valence electronic states (Fig. 5). The above XPS data indicate that the chemical stableness of the novel $K_{0.4}Rb_{0.6}Pb_2Cl_5$ crystal surface is similar to that of the ternary KPb_2Cl_5 chloride. Therefore, in spite of the fact that the $K_{0.4}Rb_{0.6}Pb_2Cl_5$ crystal contains lead, a rather hazardous chemical element, its surface is rather stable and, by analogy with its ternary counterpart KPb_2Cl_5, the crystal can be successfully used in similar technological application.

Tacking into account the possibility of XPS technique to bring pertinent information for evaluating the peculiarities of the ionic constituent of the chemical bonds in solids [48], it is interesting to compare charge transfer between lead/potassium and chlorine atoms when substituting in KPb_2Cl_5 part of K atoms by Rb atoms leading to formation of $K_{0.4}Rb_{0.6}Pb_2Cl_5$. Therefore, in Table 4 we present data of XPS measurements of core-level electrons related to the atoms composing the KPb_2Cl_5 crystal [23] that were performed using the same equipment and experimental conditions as we use in the present work for the

Table 4
Binding energies (in eV*) as established for core-level electrons associated with atoms constituting the $K_{0.4}Rb_{0.6}Pb_2Cl_5$ crystal for as-grown and bombarded with 3000 eV Ar^+ ions surfaces.

Core-level	$K_{0.4}Rb_{0.6}Pb_2Cl_5$ (as-grown surface)	$K_{0.4}Rb_{0.6}Pb_2Cl_5$ (irradiated with Ar^+ ions surface)	KPb_2Cl_5 (as-grown surface)
Pb $5d_{5/2}$	19.79	19.83	19.60
Pb $5d_{3/2}$	22.39	21.40	22.13
Pb $4f_{7/2}$	138.86	138.79	138.66
Pb $4f_{5/2}$	143.69	143.65	143.51
Cl $2p_{3/2}$	197.84	197.99	197.56
Rb $3p_{3/2}$	237.68	237.73	
Rb $3p_{1/2}$	246.63	246.66	
Cl 2s	268.89	269.00	268.60
K $2p_{3/2}$	292.65	292.74	292.46
K $2p_{1/2}$	295.36	295.41	295.15
Pb $4d_{5/2}$**	413.67	413.51	413.44
Pb $4d_{3/2}$**	435.98	435.87	435.68

Note: measurement accuracy is either ±0.05 eV* or ±0.08 eV**.

$K_{0.4}Rb_{0.6}Pb_2Cl_5$ crystal. As recommended in the case of determining the ionic component of the chemical bonds in solids [48,49], we have calculated for the $K_{0.4}Rb_{0.6}Pb_2Cl_5$ crystal the difference parameters Δ_{Pb} and Δ_K defined as differences of the BE values of core-level Pb $4f_{7/2}$ and Cl $2p_{3/2}$ spectra as well as K $2p_{3/2}$ and Cl $2p_{3/2}$ spectra, respectively. The present estimations of the XPS data indicate that $\Delta_{Pb} = -58.98 \pm 0.05$ and $\Delta_K = 94.81 \pm 0.05$ eV. These difference parameters are close to those that can be determined using the data of XPS measurements of the KPb_2Cl_5 crystal [23], in fact $\Delta_{Pb} = -58.90 \pm 0.05$ and $\Delta_K = 94.90 \pm 0.05$ eV. This implies that the ionic components of the Pb–Cl and K–Cl bonds do not change in the sequence $KPb_2Cl_5 \rightarrow K_{0.4}Rb_{0.6}Pb_2Cl_5$. This fact can be explained by that, potassium and rubidium belong to the same group of the Periodic Table.

4.3. Electronic band-structure of $K_{0.5}Rb_{0.5}Pb_2Cl_5$

The detailed information on the peculiarities of occupation of the valence-band and conduction-band regions by electronic states associated with the constituent atoms of the $K_{0.4}Rb_{0.6}Pb_2Cl_5$ crystal can be derived based on first-principles calculations of DOS. In Fig. 6, we present total DOS curves of model $K_{0.5}Rb_{0.5}Pb_2Cl_5$ solid solution as derived employing different approaches. From this figure, it is apparent that the shapes of total DOS calculating with different techniques for XC potential are quite different. To find the finest correspondence of the theory and experiment, we have plotted in Fig. 6 also the experimental XPS spectrum recorded for the valence-band area of the $K_{0.4}Rb_{0.6}Pb_2Cl_5$ crystal, for comparison.

As can be noted from Fig. 6, all the approaches used here for XC potential bring similar shapes of the basic part of the valence band of $K_{0.5}Rb_{0.5}Pb_2Cl_5$ ranging from 0 to −3.3 eV (within the energy region restricted by the formation of peculiarities A and B). However, the GGA-PBE approach gives the energy position of the sub-band C shifted by about 0.8 eV in the direction opposite to the position of the Fermi energy, E_F, as compared to that obtained employing the TB-mBJ technique. Furthermore, energy positions of the sub-bands related to Pb 5d and Rb 4p states are underestimated by about 2 eV, while that of K 3p states by about 3 eV, in comparison with the experiment. The application of the TB-mBJ model reduces those differences by about 0.2–0.3 eV. However, the most essential effect of these two models is the energy band gap value. As can be noted from calculating data listed in Table 5, the GGA-PBE model gives $E_g = 3.635$ eV for $K_{0.5}Rb_{0.5}Pb_2Cl_5$, while in the case of the TB-mBJ model we derive $E_g = 4.726$ eV. Therefore, we detect the difference of 1.1 eV in determination of the band gap value by employing those models.

The effect of underestimation of energy band gaps in band-structure

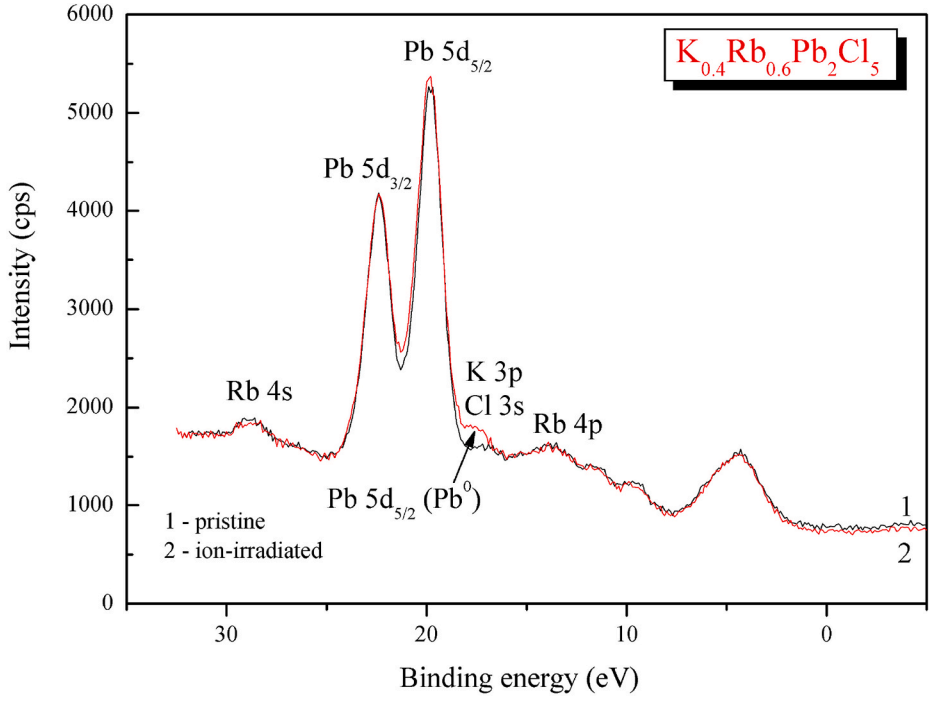

Fig. 5. Valence-band XPS spectra of the $K_{0.4}Rb_{0.6}Pb_2Cl_5$ crystal: (1) initial surface and (b) Ar^+-ion-irradiated surface.

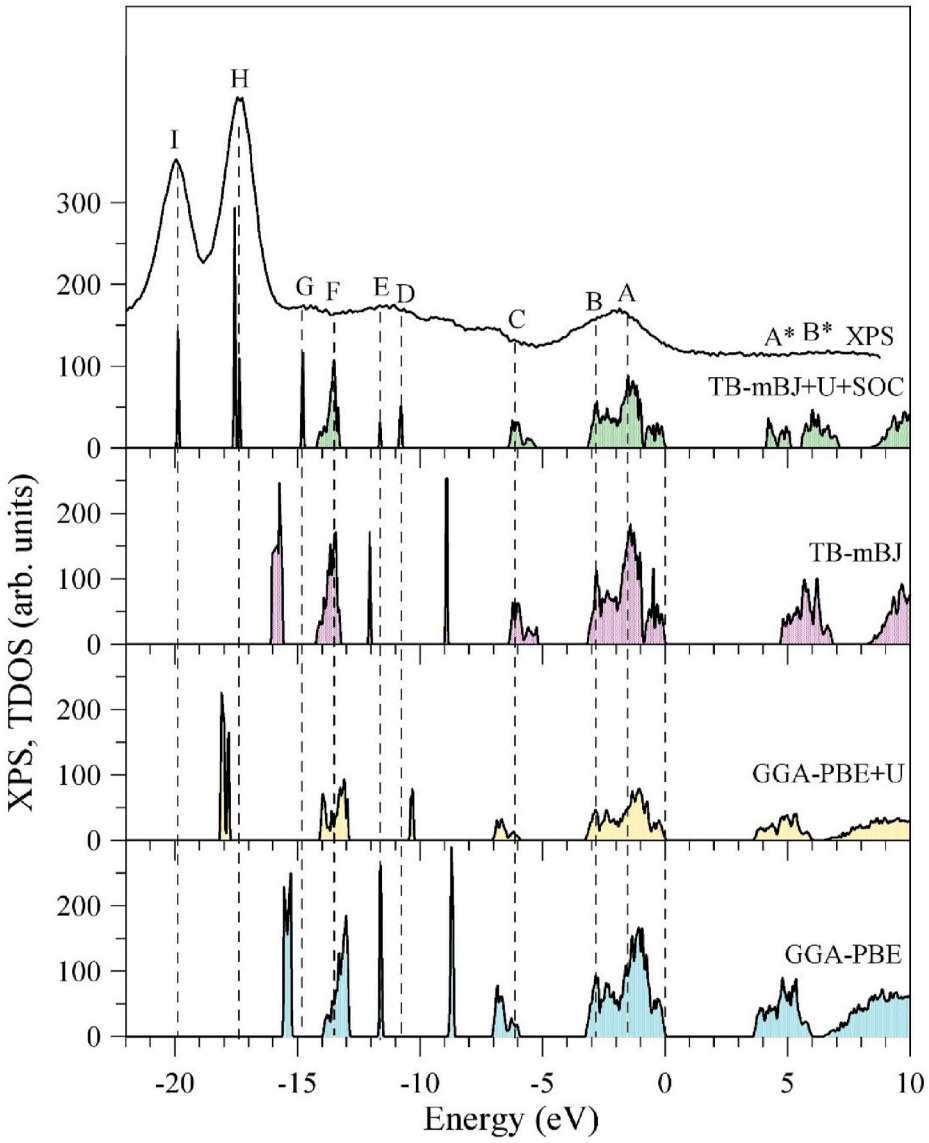

Fig. 6. Total DOS curves of $K_{0.5}Rb_{0.5}Pb_2Cl_5$ derived by DFT calculations within GGA-PBE, GGA-PBE + U, TB-mBJ, and TB-mBJ + U + SOC approaches (It should be noted that, the XPS spectrum of the $K_{0.4}Rb_{0.6}Pb_2Cl_5$ crystal is presented, for comparison, with the aim of finding the finest agreement of the theoretical data with the experiment).

Table 5
Theoretical energy band gaps of $K_{0.5}Rb_{0.5}Pb_2Cl_5$.

Method	E_g theory (eV)	E_g experiment (eV)
GGA-PBE	3.635	4.79 eV (KPb_2Cl_5)[a] [21]
GGA-PBE + U	3.644	4.83 eV ($RbPb_2Cl_5$)[a] [21]
TB-mBJ	4.726	
TB-mBJ + U + SOC	4.167	

[a] Measurements at 8 K

calculations of semiconductors and insulators when employing GGA-PBE technique is caused by overdelocalization of the occupied valence states that move the valence band toward upper energies (Fig. 7). Therefore, for heavy elements consisting d- and f-electrons, it is advantageous to apply the so-called Hubbard parameter U giving potential favoring relocalization of the occupied states to smaller energies as they are detected experimentally [50]. Following our previous finding for the best correspondence of the theoretical and experimental data regarding the occupation of the valence and semi-core electronic states [23,31], we use again the U parameter of 0.43 Ry for Pb 5d, K 3p and Rb 4p electrons. As can be seen from Fig. 6, the application of the above-indicated Hubbard parameter U shifts the sub-bands associated with Pb 5d, K 3p and Rb 4p electrons away from the Fermi level by about 2.0–2.3 eV resulting in a much better fit of the theoretical data with the experiment. However, the use of the Hubbard parameter U in the above calculations almost does not alter the E_g value of the $K_{0.5}Rb_{0.5}Pb_2Cl_5$ compound (Table 5). The best agreement with the XPS valence-band spectrum we observe when applying the TB-mBJ approach, which includes the Hubbard parameter U as well as the effect of SOC (TB-mBJ + U + SOC model). The inducing exchange interaction between p and d orbitals of the localized electronic states and the conduction band in such a case brings to the band overlapping resulting in the decrease of energy band gap of $K_{0.5}Rb_{0.5}Pb_2Cl_5$ by 0.559 eV in comparison with that obtained in the calculations within the TB-mBJ model (Table 5). Importantly, the separation of the Pb $5d_{3/2}$ and Pb $5d_{5/2}$ electronic states as determined in the present band-structure calculations within the TB-mBJ + U + SOC model is equal to 2.4 eV that is in fairly good agreement with the experimental determination by XPS of the spin-orbit coupling of these electronic states (Table 4).

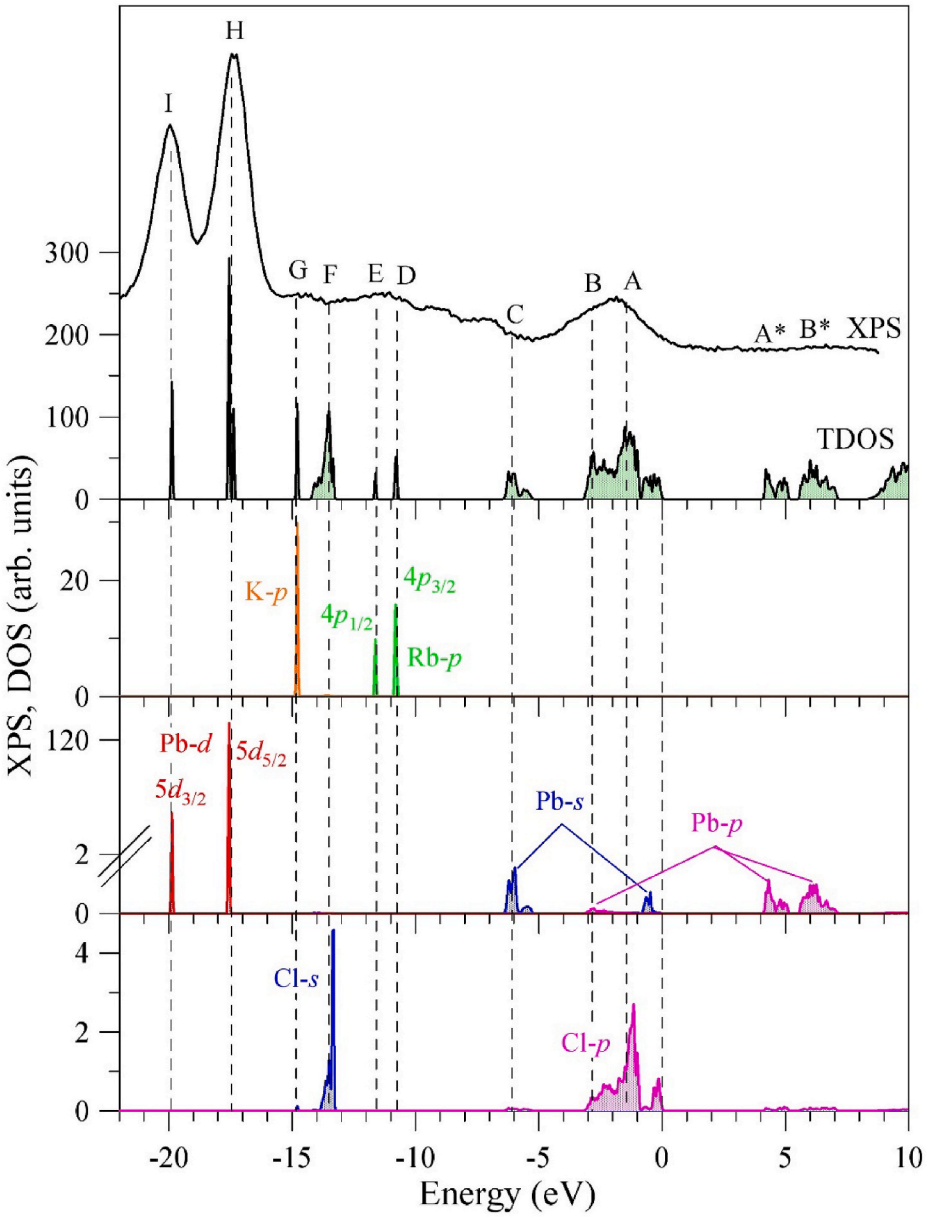

Fig. 7. Total and partial DOS curves of $K_{0.5}Rb_{0.5}Pb_2Cl_5$ derived in our DFT calculations within the TB-mBJ + U + SOC model (It should be noted that, the XPS spectrum of the $K_{0.4}Rb_{0.6}Pb_2Cl_5$ crystal is presented, for comparison).

The data of DFT calculations of partial DOS curves of $K_{0.5}Rb_{0.5}Pb_2Cl_5$ carried out applying the TB-mBJ + U + SOC approach are presented in Fig. 7 bringing important information regarding occupation of the valence band and the conduction band by electronic states of special symmetry for the constituent atoms. As can be noted from Fig. 7, the main part of the valence band of $K_{0.5}Rb_{0.5}Pb_2Cl_5$ is determined by the input of Cl 3p states providing the main contribution in its central portion with the smaller contribution of Pb s and Pb p states in its upper and lower portions, respectively. The bottom of the sub-band B is separated from the top of the sub-band C by a 2.1 eV energy gap. The sub-band C, which ranges from −5.2 to −6.4 eV and centered at −6.1 eV is formed principally from Pb 6s states with smaller contributions from Cl 3p states, too. The narrow sub-bands D and E centered at about −10.8 and −11.6 eV are due to inputs of Rb $5p_{3/2}$ and Rb $5p_{1/2}$ states, respectively, while the sub-bands centered at about −13.5 and −14.4 eV are originated from Cl 3s and K 4s states, respectively. Further, Pb $5d5_{/2}$ and Pb $5d_{3/2}$ states form strong sub-bands centered at about −17.5 and −19.9 eV, respectively. The bottom of the conduction band (sub-band A* spreading from 4.2 to 5.3 eV) is composed by unoccupied Pb 6p states with smaller contributions of Cl 3p* states, too. The same origin is characteristic for the upper sub-band B* of the conduction band ranging from 5.6 to 7.2 eV. From Fig. 7, it is obvious that electronic states associated with potassium and rubidium atoms give very minor contributions to the valence band and conduction band of $K_{0.5}Rb_{0.5}Pb_2Cl_5$. Very minor contributions of electronic states by K and/or Rb atoms in those bands were found to be characteristic for related chloride KPb_2Cl_5 [23] and bromides $K_{0.5}Rb_{0.5}Pb_2Br_5$ [31], KPb_2Br_5 [32], and $RbPb_2Br_5$ [50]. Additionally, the main peculiarities of the energy distribution of densities of electronic states of Pb 6s(6p) and/or Rb 4p/(Cl 3p/Br 4p) symmetries in the valence band and the conduction band of those chlorides and bromides look to be similar to those of Pb 6s(6p) and Rb 4p/Cl 3p electronic states of $K_{0.5}Rb_{0.5}Pb_2Cl_5$. Furthermore, as data presented in Fig. 7 reveal, we detect small hybridization of Cl 3p states with Pb 6s states at the top and near the bottom of the valence band. Therefore, the nature of the chemical Pb–Cl bonds in $K_{0.5}Rb_{0.5}Pb_2Cl_5$ is mainly ionic because the covalent component of the chemical bonding

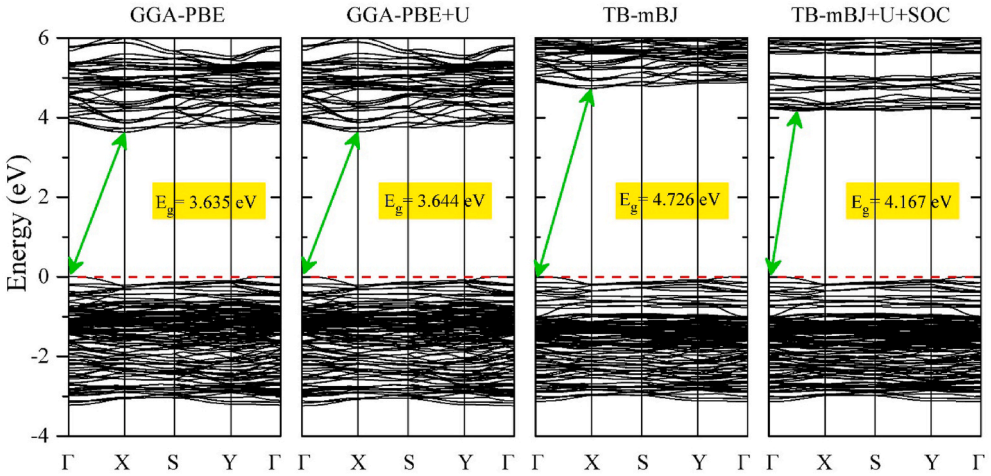

Fig. 8. Bands dispersion through high symmetry points of the first Brillouin zone with monoclinic structure of $K_{0.5}Rb_{0.5}Pb_2Cl_5$ obtained in our DFT calculations within the GGA-PBE, GGA-PBE + U, TB-mBJ, and TB-mBJ + U + SOC approaches.

in this solid solution is rather small. Previously, for related thallium-bearing chloride $TlPb_2Cl_5$, it was established that the chemical Pb–Cl bonds are mainly of covalent nature [51].

Results of our DFT calculations of bands dispersion of $K_{0.5}Rb_{0.5}Pb_2Cl_5$ through high symmetry points of the first Brillouin zone with monoclinic structure within the GGA-PBE, GGA-PBE + U, TB-mBJ, and TB-mBJ + U + SOC approaches are presented in Fig. 8. All these approaches bring to the conclusion that $K_{0.5}Rb_{0.5}Pb_2Cl_5$ is an indirect band gap material. However, some differences depending on the choice of the model are obvious. Applications of all the models for XC potential indicate that maximum of the valence band is positioned at Γ point, and minimum values for the conduction band are detected at X point due to the calculations within the GGA-PBE, GGA-PBE + U, and TB-mBJ models, while the applying of the TB-mBJ + U + SOC approach reveals that minimum value of the conduction band is located at the k point positioned somewhere near the middle of the Γ–X direction. These results present the significance of the consideration of SOC effect in DFT calculations. The same conclusion was made recently when clarifying peculiarities of the electronic structure of Tl_4PbI_6 halide [52] by employing different models including and ignoring SOC effect. As can be noted from Fig. 8, dispersions of the bands in the vicinities of the valence band maximum and the conduction band minimum of $K_{0.5}Rb_{0.5}Pb_2Cl_5$ are rather flat suggesting high values of effective mass and low values of mobility of electron in this complex chloride.

4.4. Optical constants of $K_{0.5}Rb_{0.5}Pb_2Cl_5$

It is well-known that optical constants can be derived theoretically based on DFT band-structure calculations [53]. By using the Kramers-Kronig relations [45], the real and imaginary components of the dielectric function, $\varepsilon_1(\omega)$ and $\varepsilon_2(\omega)$, respectively, can be derived theoretically using formula involving the Fermi distribution function (f_{kn}) of a crystal, volume of its unit-cell (V), eigenvalue energy (E_{kn}) of the wave function ($|kn\sigma\rangle$), crystal's momentum (k) and spin (σ) [54]:

$$\varepsilon_2^{ij}(\omega) = \frac{4\pi^2 e^2}{Vm^2\varpi^2} \times \sum_{nn'\sigma} \langle kn\sigma|p_i|kn'\sigma\rangle \langle kn'\sigma\left|p_j\right|kn\rangle \times f_{kn}(1-fkn')\delta(E_{kn'} - E_{kn} - h\omega)$$

$$\varepsilon_1(\omega) = 1 + \frac{2}{\pi} P \int_0^{\infty} \frac{\omega' \varepsilon_2(\omega')}{\omega' 2 - \omega^2} d\omega'$$

where P, m, e, ω, and p are Cauchy's principal value, mass of electron and its charge, penetrating electromagnetic wave frequency, and the momentum operator, respectively. The results of calculations of the real and imaginary components of the dielectric function, $\varepsilon_1(\omega)$ and $\varepsilon_2(\omega)$, respectively, for $K_{0.5}Rb_{0.5}Pb_2Cl_5$ are presented in Fig. 9. As can be noted from Fig. 9a, the $\varepsilon_1(\omega)$ function increases beginning from 0 eV and reaches its maximum A near 4.45 eV. With further enhancing photon energies, the $\varepsilon_1(\omega)$ function goes down revealing features B (at 5.75 eV) and C (at 6.79 eV) till its minimum positioned around 8 eV. Further

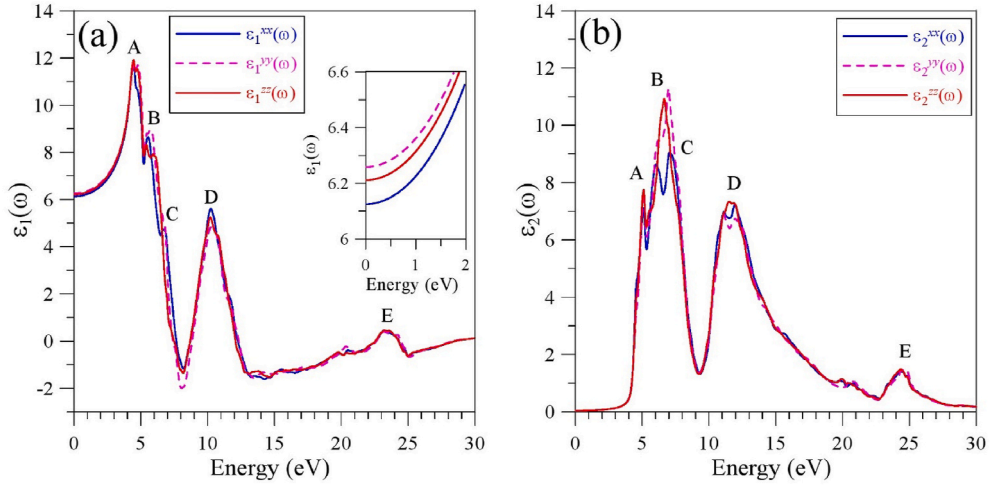

Fig. 9. (a) Real $\varepsilon_1(\omega)$ and (b) imaginary $\varepsilon_2(\omega)$ constituents of dielectric function of $K_{0.5}Rb_{0.5}Pb_2Cl_5$ as derived within the TB-mBJ + U + SOC model.

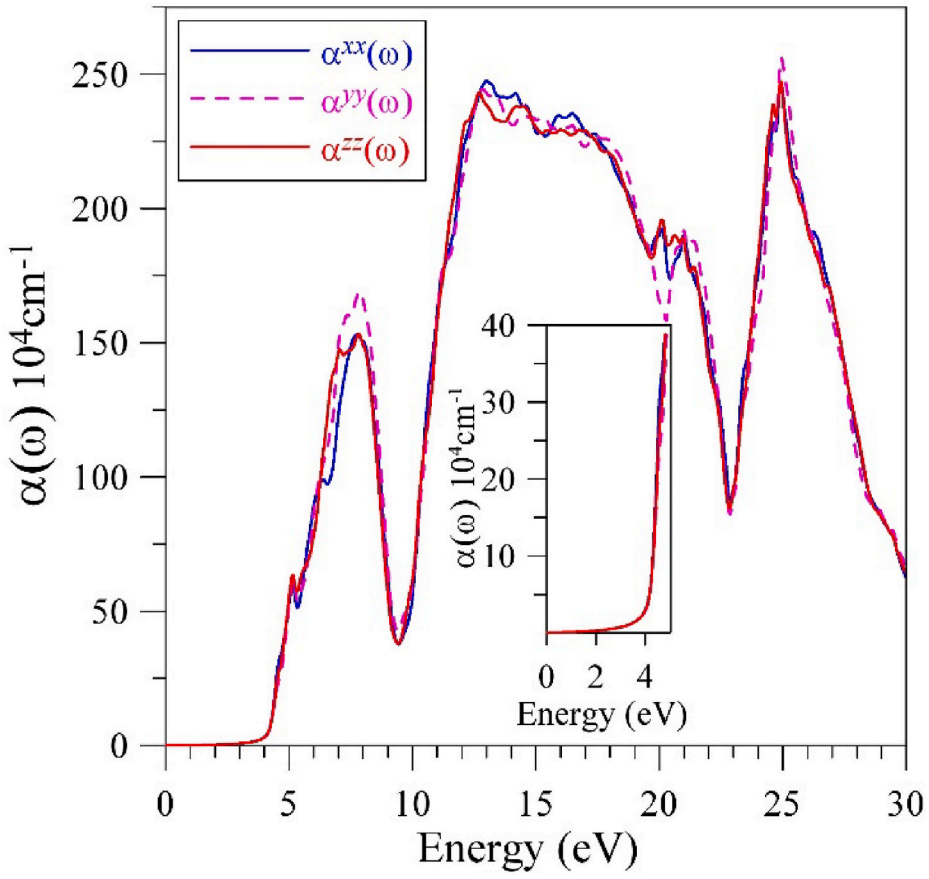

Fig. 10. Absorption coefficient $\alpha(\omega)$ of $K_{0.5}Rb_{0.5}Pb_2Cl_5$ as derived within the TB-mBJ + U + SOC model.

increase of photon energies reveals the formation of a well-defined sub-band D centered at about 10.3 eV and a feature C centered at 23.3 eV. The real part $\varepsilon_1(\omega)$ of the dielectric function of $K_{0.5}Rb_{0.5}Pb_2Cl_5$ is almost isotropic in the whole calculating energy region (0–30 eV): the polarization of ${\varepsilon_1}^{xx}(\omega)$, ${\varepsilon_1}^{yy}(\omega)$, and ${\varepsilon_1}^{zz}(\omega)$ components is detected in the vicinities of the maxima/features A, B, C, and D. The static dielectric values of the real component $\varepsilon_1(\omega)$ of the dielectric function of $K_{0.5}Rb_{0.5}Pb_2Cl_5$ are following: ${\varepsilon_1}^{xx}(0) = 6.12543$, ${\varepsilon_1}^{yy}(0) = 6.25879$, and ${\varepsilon_1}^{zz}(0) = 6.21156$. Fig. 9b demonstrates that the imaginary component $\varepsilon_2(\omega)$ of the dielectric function of $K_{0.5}Rb_{0.5}Pb_2Cl_5$ reveals the presence of the features A to E in the energy regions corresponding to those detected for the similar features of the $\varepsilon_1(\omega)$ function, in fact, A (~5.1 eV), B (~6.6 eV), C (~7.3 eV), D (~11.5 eV), and E (~24.3 eV). The maximum values of the imaginary component $\varepsilon_2(\omega)$ of the dielectric function of $K_{0.5}Rb_{0.5}Pb_2Cl_5$ are detected for energies ranging from 5 till 7 eV that relate to near ultraviolet region. The $\varepsilon_2(\omega)$ function presents essential anisotropy near the maximum/peculiarity B.

Such important optical constants as the adsorption coefficient $\alpha(\omega)$, refraction index $n(\omega)$, extinction coefficient $k(\omega)$, energy loss spectrum $L(\omega)$ and optical reflectance $R(\omega)$ of $K_{0.5}Rb_{0.5}Pb_2Cl_5$ can be calculated using following equations [53]:

$$\alpha^{ij}(\omega) = \frac{2\omega k^{ij}(\omega)}{c}$$

$$n^{ij}(\omega) = \frac{1}{\sqrt{2}}\left[\sqrt{\varepsilon_1^{ij}(\omega)^2 + \varepsilon_2^{ij}(\omega)^2} + \varepsilon_1^{ij}(\omega)\right]^{1/2}$$

$$k^{ij}(\omega) = \frac{1}{\sqrt{2}}\left[\sqrt{\varepsilon_1^{ij}(\omega)^2 + \varepsilon_2^{ij}(\omega)^2} - \varepsilon_1^{ij}(\omega)\right]^{1/2}$$

$$L^{ij}(\omega) = -\mathrm{Im}\left(\varepsilon^{-1}\right)^{ij} = \frac{\varepsilon_2^{ij}(\omega)}{\varepsilon_1^{ij}(\omega)^2 + \varepsilon_2^{ij}(\omega)^2}$$

$$R^{ij}(\omega) = \frac{(n^{ij}-1)^2 + k^{ij2}}{(n^{ij}+1)^2 + k^{ij2}} = \left|\frac{\sqrt{\varepsilon_1^{ij} + i\varepsilon_2^{ij}} - 1}{\sqrt{\varepsilon_1^{ij} + i\varepsilon_2^{ij}} + 1}\right|^2$$

From Fig. 10, where results of our calculations of the absorption coefficient $\alpha(\omega)$ of $K_{0.5}Rb_{0.5}Pb_2Cl_5$ are presented, one can see that the first critical point arises near 4.2 eV. The $\alpha(\omega)$ function reveals three well-defined sub-bands: first one being in the energy range from 4.2 till about 9.5 eV, the second one ranging from 9.5 up to about 23 eV, and above this energy value the formation of the third sub-band of the absorption coefficient $\alpha(\omega)$ is detected. It is worth mentioning that in a comparatively wide energy region, at least from about 5 eV till 30 eV, the $\alpha(\omega)$ function reveals values of above 10^5 cm-1. Therefore, the $K_{0.5}Rb_{0.5}Pb_2Cl_5$ compound possesses high absorption in the energy range covering a region of electromagnetic waves from middle ultraviolet till vacuum ultraviolet. This means, that $K_{0.5}Rb_{0.5}Pb_2Cl_5$ can find application in optoelectronic devices.

Our calculations indicate that the refractive index $n(\omega)$ of $K_{0.5}Rb_{0.5}Pb_2Cl_5$ and its extinction coefficient $n(\omega)$ possess some similarities with the real $\varepsilon_1(\omega)$ and imaginary $\varepsilon_2(\omega)$ components of the dielectric function, respectively (cf. Figs. 9 and 11 (a and b)). Our data allow for statement that static values of the refractive index of $K_{0.5}Rb_{0.5}Pb_2Cl_5$ are following: ${n}^{xx}(0) = 2.47497$, ${n}^{yy}(0) = 2.50177$, and ${n}^{zz}(0) = 2.49231$. Beginning from those values, the refractive index $n(\omega)$ increases to the highest values observed for photon energies of 3–6 eV, where some anisotropy for the second rank tensor constituents ${n}^{xx}(\omega)$, ${n}^{yy}(\omega)$ and ${n}^{zz}(\omega)$ is visible. Further, the extinction coefficient $k(\omega)$

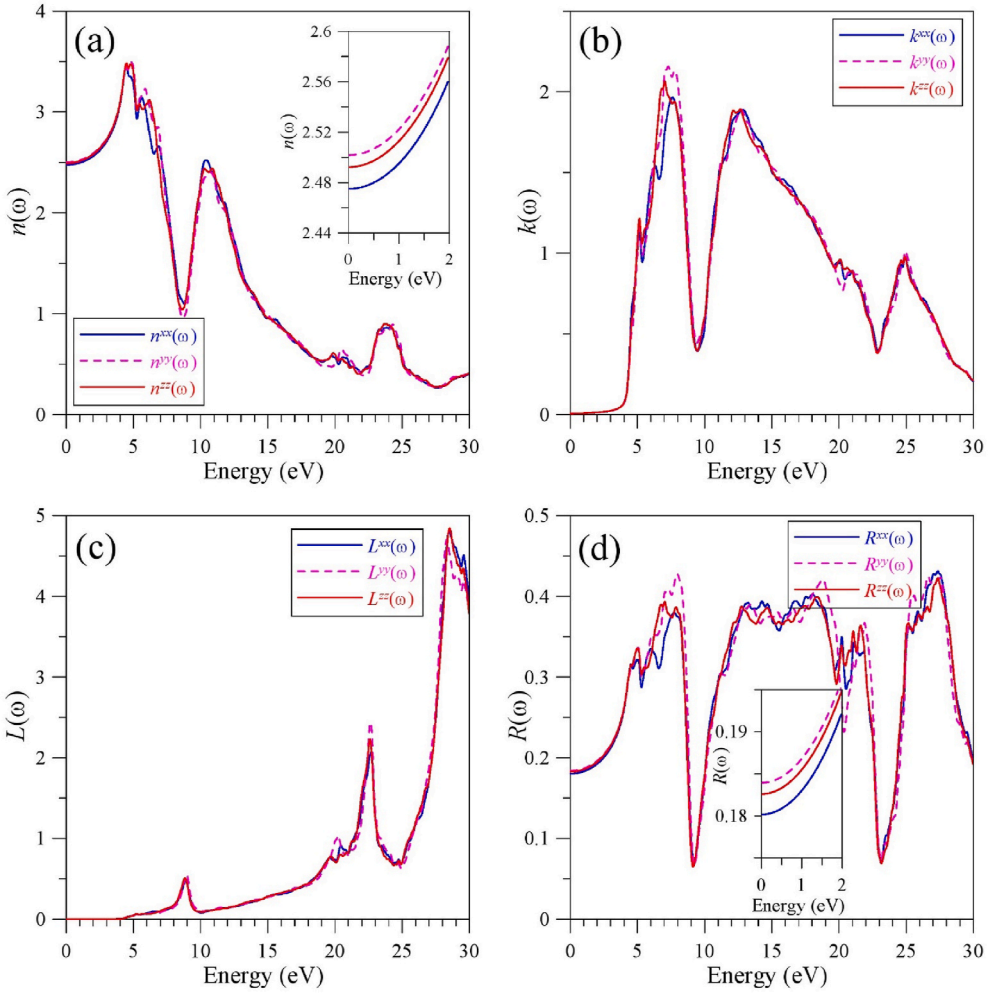

Fig. 11. (a) Refractive index $n(\omega)$, (b) extinction coefficient $k(\omega)$, (c) electron energy-loss spectrum $L(\omega)$, (d) optical reflectivity $R(\omega)$ of $K_{0.5}Rb_{0.5}Pb_2Cl_5$ as derived within the TB-mBJ + U + SOC model.

presents some anisotropy behavior of the $k^{xx}(\omega)$, $k^{yy}(\omega)$ and $k^{zz}(\omega)$ components for photon energies of 6–7.5 eV. As can be seen from Fig. 11c, the energy-loss spectrum $L(\omega)$ reveals the formation of a sub-band centered at about 22.5 eV which is associated with the plasma oscillation in $K_{0.5}Rb_{0.5}Pb_2Cl_5$. Calculated coefficient of optical reflectivity $R(\omega)$ of $K_{0.5}Rb_{0.5}Pb_2Cl_5$ (Fig. 11d) presents that the biggest reflectivity values (bigger than 35%) are detected for photons in the energy region of about 6–8.5, 12–20, and 25–28 eV, where anisotropic behavior of the second rank components $R^{xx}(\omega)$, $R^{yy}(\omega)$, and $R^{zz}(\omega)$ is observed with static coefficients $R^{xx}(0) = 18.02\%$, $R^{yy}(0) = 18.39\%$, and $R^{zz}(0) = 18.26\%$. All the above data of calculations of the optical constants allow for the statement that $K_{0.5}Rb_{0.5}Pb_2Cl_5$ is a prospective optoelectronic material.

5. Conclusions

Optical quality $K_{0.4}Rb_{0.6}Pb_2Cl_5$ crystal was successfully grown by Bridgman method and its crystal structure and the electronic and optical properties were studied in detail. The present single crystal X-ray diffraction measurements indicate that the $K_{0.4}Rb_{0.6}Pb_2Cl_5$ crystal possesses a monoclinic unit cell (SG $P2_1/c$) with the unit-cell parameters as follows: a = 8.9484(2) Å, b = 7.9802(2) Å, c = 12.5359 Å, and β = 90.1220(10)°. Our XPS experiments demonstrate very low hygroscopicity of the $K_{0.4}Rb_{0.6}Pb_2Cl_5$ crystal surface and its partial transformation of Pb^{2+} ions to Pb^0 when irradiating with middle-energy Ar^+ ions. The present XPS data indicate that the chemical stableness of the novel $K_{0.4}Rb_{0.6}Pb_2Cl_5$ crystal surface is similar to that of the ternary KPb_2Cl_5 chloride. Therefore, in spite of the fact that the $K_{0.4}Rb_{0.6}Pb_2Cl_5$ crystal contains a rather hazardous chemical element, lead, its surface is rather stable and, by analogy with its ternary counterpart KPb_2Cl_5, the crystal can be successfully used in similar technological application. When comparing with the similar XPS measurements of the related KPb_2Cl_5 chloride [23], we detect that the ionic components of the Pb–Cl and K–Cl bonds do not change in the sequence $KPb_2Cl_5 \rightarrow K_{0.4}Rb_{0.6}Pb_2Cl_5$.

To explore peculiarities of filling the valence band and the conduction band of the crystal under consideration by partial electronic states related to the constituent atoms, we have applied various approaches for XC potential using model $K_{0.5}Rb_{0.5}Pb_2Cl_5$ solid solution. The present theoretical findings allow for the statement that the finest agreement of the experimental and theoretical data is observed when employing the TB-mBJ + U + SOC approach. The DFT calculating data within the TB-mBJ + U + SOC model present that the main part of the valence band of $K_{0.5}Rb_{0.5}Pb_2Cl_5$ is determined by contributions of Cl 3p states giving the main input in its central portion with smaller contributions of Pb s and Pb p states in its upper and lower parts, respectively. The sub-band near the main part of the valence band of $K_{0.5}Rb_{0.5}Pb_2Cl_5$ is originated mainly from Pb 6s states with smaller input of Cl 3p states, too. The conduction band bottom is formed mainly by unoccupied Pb 6p states with smaller contributions of unoccupied Cl 3p states as well. We detect rather small hybridization of Cl 3p states with Pb 6s states at the top and near the bottom of the valence band. Therefore, the nature of the chemical Pb–Cl bonds in $K_{0.5}Rb_{0.5}Pb_2Cl_5$ is mainly ionic because the covalent

constituent of the chemical bonding in this solid solution is rather small. The bands dispersions in the vicinities of maximum of the valence band and minimum of the conduction band are rather flat suggesting high values of effective mass and low values of mobility of electron in $K_{0.5}Rb_{0.5}Pb_2Cl_5$. The present DFT calculations predict that $K_{0.5}Rb_{0.5}Pb_2Cl_5$ is a non-direct material with energy band gap of 4.167 eV.

The optical properties of $K_{0.5}Rb_{0.5}Pb_2Cl_5$ are elucidated theoretically in detail based on first-principles calculations applying the TB-mBJ + U + SOC model. In particular, we have detected that the real part $\varepsilon_1(\omega)$ of the dielectric function of $K_{0.5}Rb_{0.5}Pb_2Cl_5$ is almost isotropic in the whole calculating energy region (0–30 eV) where the polarization of $\varepsilon_1{}^{xx}(\omega)$,$\varepsilon_1{}^{yy}(\omega)$, and $\varepsilon_1{}^{zz}(\omega)$ components is detected in the vicinities of some maxima/features. The static dielectric constants of the $\varepsilon_1(\omega)$ function of $K_{0.5}Rb_{0.5}Pb_2Cl_5$ are following: $\varepsilon_1{}^{xx}(0) = 6.12543$, $\varepsilon_1{}^{yy}(0) = 6.25879$, and $\varepsilon_1{}^{zz}(0) = 6.21156$. The calculations of the absorption coefficient $\alpha(\omega)$ present that, the first critical point in $K_{0.5}Rb_{0.5}Pb_2Cl_5$ arises near 4.2 eV. In a comparatively wide energy region, at least from about 5 eV till 30 eV, the $\alpha(\omega)$ function reveals values of above 10^5 cm-1. Therefore, the $K_{0.5}Rb_{0.5}Pb_2Cl_5$ compound possesses high absorption behavior in the energy range covering a region of electromagnetic waves from middle ultraviolet till vacuum ultraviolet. The refractive index $n(\omega)$ and extinction coefficient $n(\omega)$ possess some similarities with the real and imaginary components of the dielectric function, $\varepsilon_1(\omega)$ and $\varepsilon_2(\omega)$, respectively. The static values of the refractive index of $K_{0.5}Rb_{0.5}Pb_2Cl_5$ are equal to $n^{xx}(0) = 2.47497$, $n^{yy}(0) = 2.50177$, and $n^{zz}(0) = 2.49231$. The energy-loss spectrum $L(\omega)$ reveals the presence of a sub-band centered around 22.5 eV which is associated with the plasma oscillation in $K_{0.5}Rb_{0.5}Pb_2Cl_5$. Calculated coefficient of optical reflectivity $R(\omega)$ of $K_{0.5}Rb_{0.5}Pb_2Cl_5$ presents that the biggest reflectivity values (bigger than 35%) are detected for photons in the energy region of about 6–8.5, 12–20, and 25–28 eV. Our data indicate that $K_{0.5}Rb_{0.5}Pb_2Cl_5$ is a promising material for the use in optoelectronic devices.

CRediT authorship contribution statement

O.Y. Khyzhun: Writing – original draft, Writing – review & editing, Supervision. **Tuan V. Vu:** Methodology, Investigation. **A.A. Lavrentyev:** Data curation, Conceptualization, Formal analysis. **B.V. Gabrelian:** Data curation, Visualization. **N.M. Denysyuk:** Data curation, Investigation. **L.I. Isaenko:** Writing – original draft, Investigation. **M.S. Molokeev:** Data curation, Investigation. **A.A. Goloshumova:** Investigation, Validation. **A.Y. Tarasova:** Data curation, Investigation.

Declaration of competing interest

The authors declare that they have no known competing financial interests or personal relationships that could have appeared to influence the work reported in this paper.

Acknowledgments

This work was supported by the Ministry of Education and Science of the Russian Federation, grant FSUS-2020-0036, and was partly performed on the state assignment of IGM SB RAS. The X-ray single crystal data were derived using the analytical equipment of Krasnoyarsk Regional Center of Research Equipment of Federal Research Center "Krasnoyarsk Science Center SB RAS".

References

[1] M. Velázquez, A. Ferrier, J.-L. Doualan, R. Moncorgé, in: A.H. Al-Khursan (Ed.), Solid State Laser, InTech, Rijeka, Croatia, 2012, pp. 119–142.
[2] C.W. Hoyt, M.P. Hasselbeck, M. Sheik-Bahae, R. Epstein, C. Greenfield, J. Thiede, J. Distel, J. Valencia, J. Opt. Soc. Am. B 20 (2003) 1066–1074.
[3] K. Rademaker, E. Neumann, G. Huber, S.A. Payne, W.F. Krupke, L.I. Isaenko, A. Burger, Opt. Lett. 30 (7) (2005) 729–731.
[4] A.G. Bluiett, N.J. Condon, S. O'Connor, S.R. Bowman, M. Logie, J. Ganem, J. Opt. Soc. Am. B 22 (10) (2005) 2250–2256.
[5] P. Amedzake, E. Brown, U. Hömmerich, S.B. Trivedi, J.M. Zavada, J. Cryst. Growth 310 (2008) 2015–2019.
[6] A. Ferrier, M. Velázquez, J.-L. Doulan, R. Moncorgé, J. Lumin. 129 (2009) 1905–1907.
[7] Y. Tian, R. Xu, L. Zhang, L. Hu, J. Zhang, J. Appl. Phys. 108 (2010), 083504.
[8] M. Piasecki, G. Lakshminarayana, A.O. Fedorchuk, O.S. Kushnir, V.A. Franiv, A. V. Franiv, G. Myronchuk, K.J. Plucinski, J. Mater. Sci. Mater. Electron. 24 (2013) 1187–1193.
[9] A.M. Tkachuk, S.E. Ivanova, L.I. Isaenko, A.P. Yelisseyev, M.-F. Jubert, Y. Guyot, S. Payne, Opt Spectrosc. 95 (2003) 722–740.
[10] R. Balda, J. Fernandez, A. Mendioroz, M. Voda, M. Al-Saleh, Opt. Mater. 24 (2003) 91–95.
[11] N.W. Jenkins, S.R. Bowman, S. O'Connor, S.K. Searles, J. Ganem, Opt. Mater. 22 (2003) 311–320.
[12] A.J. Garcia-Adeva, R. Balda, J. Fernández, E.E. Nyein, U. Hömmerich, Phys. Rev. B 72 (2005) 165116.
[13] U. Hömmerich, E.E. Nyein, J.A. Freeman, P. Amedzake, S.B. Trivedi, J.M. Zavada, J. Cryst. Growth 287 (2006) 230–233.
[14] R.S. Quimby, N.J. Condon, S.P. O'Connor, S. Biswal, S.R. Bowman, Opt. Mater. 30 (2008) 827–834.
[15] A.G. Bluiett, D. Peele, K. Norman, E. Brown, U. Hömmerich, S.B. Trivedi, J. M. Zavada, Opt. Mater. 33 (2011) 985–988.
[16] M. Sobczyk, J. Dozdzynski, R. Lisiecki, W. Ryba-Romanowski, Opt. Mater. 29 (2007) 1029–1034.
[17] R. Balda, J. Fernandez, A. Mendioroz, M. Voda, M. Al-Saleh, Phys. Rev. B 68 (2003) 165101.
[18] G. Jia, H. Wang, C. Wang, S. Zhao, D. Deng, L. Huang, Y. Hua, C. Li, S. Xu, J. Alloys Compd. 509 (2011) 8365–8369.
[19] L. Isaenko, A. Yelisseyev, A. Tkachuk, S. Ivanova, S. Vatnik, A. Merkulov, S. Payne, R. Page, M. Nostrand, Mater. Sci. Eng. B 81 (2001) 188–190.
[20] A. Merkulov, L.I. Isaenko, V.M. Pashkov, V.G. Mazur, A.V. Virovets, D.Yu Naumov, J. Struct. Chem. 46 (2005) 103–108.
[21] L.I. Isaenko, I.N. Ogorodnikov, V.A. Pustovarov, A.Y. Tarasova, V.M. Pashkov, Opt. Mater. 35 (2013) 620–625.
[22] A.H. Reshak, O.Y. Khyzhun, I.V. Kityk, A.O. Fedorchuk, H. Kamarudin, S. Auluck, O.V. Parasyuk, Sci. Adv. Mater. 5 (2013) 316–327.
[23] T.V. Vu, A.A. Lavrentyev, B.V. Gabrelian, D.D. Vo, K.D. Pham, N.M. Denysyuk, L. I. Isaenko, A.Y. Tarasova, O.Y. Khyzhun, Opt. Mater. 102 (2020) 109793.
[24] N.V. Lichkova, V.N. Zagorodnev, A.G. Okhrimchuk, L.N. Butvina, D.V. Irzhak, V. K. Karandashev, Inorg. Mater. 50 (2014) 194–204.
[25] SADABS, Area-Detector Absorption Correction, Siemens Industrial Automation, Inc., Madison, WI, USA, 1996.
[26] G.M. Sheldrick, Acta Crystallogr. A 64 (2008) 112–122.
[27] PLATON – A Multipurpose Crystallographic Tool, Utrecht University, Utrecht, The Netherlands, 2008.
[28] K. Brandenburg, M. Berndt, DIAMOND - Visual Crystal Structure Information System CRYSTAL IMPACT, Postfach vol. 1251, D-53002 Bonn.
[29] A.Y. Tarasova, L.I. Isaenko, V.G. Kesler, V.M. Pashkov, A.P. Yelisseyev, N. M. Denysyuk, O.Y. Khyzhun, J. Phys. Chem. Solid. 73 (2012) 674–682.
[30] P. Blaha, K. Schwarz, G.K.H. Madsen, D. Kvasnicka, J. Luitz, R. Laskowski, F. Tran, L.D. Marks, WIEN2k, An Augmented Plane Wave + Local Orbitals Program for Calculating Crystal Properties, Karlheinz Schwarz, Techn, Universitt Wien, Austria, 2018. ISBN 3-9501031-1-2.
[31] T.V. Vu, A.A. Lavrentyev, B.V. Gabrelian, D.D. Vo, H.D. Tong, N.M. Denysyuk, L. I. Isaenko, A.Y. Tarasova, O.Y. Khyzhun, RSC Adv. 10 (2020) 11156–11164.
[32] A.A. Lavrentyev, B.V. Gabrelian, V.T. Vu, N.M. Denysyuk, P.N. Shkumat, A. Y. Tarasova, L.I. Isaenko, O.Y. Khyzhun, Opt. Mater. 53 (2016) 64–72.
[33] J.P. Perdew, K. Burke, M. Ernzerhof, Phys. Rev. Lett. 77 (18) (1996) 3865–3868.
[34] F. Tran, P. Blaha, Phys. Rev. Lett. 102 (2009) 226401.
[35] D. Koller, F. Tran, P. Blaha, Phys. Rev. B 85 (2012) 155109.
[36] V.I. Anisimov, I.V. Solovyev, M.A. Korotin, M.T. Czyzyk, G.A. Sawatzky, Phys. Rev. B 48 (1993) 16929–16934.
[37] P. Novak, F. Boucher, P. Gressier, P. Blaha, K. Schwarz, Phys. Rev. B 63 (2001) 235114.
[38] D.D. Koelling, B.N. Harmon, J. Phys. C Solid State Phys. 10 (16) (1977) 3107–3114.
[39] P.B. Moore, P.K. Sen Gupta, Y. Le Page, Am. Mineral. 74 (1989) 1186–1194.
[40] P.B. Moore, P.K. Sen Gupta, S. Jinchuan, E.O. Schlemper, Am. Mineral. 76 (1991) 1389–1399.
[41] L.I. Isaenko, K.E. Korzhneva, M.S. Molokeev, A.A. Goloshumova, A.Y. Tarasova, J. Solid State Chem. 277 (2019) 786–792.
[42] S.P. Guo, Y. Chi, G.-C. Guo, Coord. Chem. Rev. 335 (2017) 44–57.
[43] Y. Kogut, O.Y. Khyzhun, O.V. Parasyuk, A.H. Reshak, G. Lakshminarayama, I. V. Kityk, M. Piasecki, J. Cryst. Growth 354 (2012) 142–146.
[44] Z.-Z. Luo, C.-S. Lin, H.-H. Cui, W.-L. Zhang, H. Zhang, H. Chen, Z.-Z. He, W.-D. Cheng, Chem. Mater. 27 (2015) 914–922.
[45] A.O. Fedorchuk, O.V. Parasyuk, O. Cherniushok, B. Andriyevsky, G.L. Myronchuk, O.Y. Khyzhun, G. Lakshminarayana, J. Jedryka, I.V. Kityk, A.M. ElNaggar, A. A. Albassam, M. Piasecki, J. Alloys Compd. 740 (2018) 294–304.
[46] M.G. Brik, I.V. Kityk, N.M. Denysyuk, O.Y. Khyzhun, S.I. Levkovets, O.V. Parasyuk, A.O. Fedorchuk, G.L. Myronchuk, Phys. Chem. Chem. Phys. 16 (2014) 12838–12847.
[47] O.Y. Khyzhun, P.M. Fochuk, I.V. Kityk, M. Piasecki, S.I. Levkovets, A.O. Fedorchuk, O.V. Parasyuk, Mater. Chem. Phys. 172 (2016) 165–172.

[48] A. Taylor, in: D. Briggs, M.P. Seah (Eds.), Practical Surface Analysis, second ed. Auger and X-Ray Photoelectron Spectroscopy, vol. 1, John Wiley, New York, 1990.
[49] S. Hufner, Photoelectron Spectroscopy: Principles and Applications, Springer-Verlag, Berlin, Heidelberg, 2003.
[50] A.A. Lavrentyev, B.V. Gabrelian, V.T. Vu, N.M. Denysyuk, P.N. Shkumat, A. Y. Tarasova, L.I. Isaenko, O.Y. Khyzhun, J. Phys. Chem. Solid. 91 (2016) 25–33.
[51] O.Y. Khyzhun, V.L. Bekenev, N.M. Denysyuk, O.V. Parasyuk, A.O. Fedorchuk, J. Alloys Compd. 582 (2014) 802–809.
[52] T.V. Vu, I.V. Luzhnyi, G.L. Myronchuk, V.L. Bekenev, M.S. Bohdanyuk, A. A. Lavrentyev, B.V. Gabrelian, O.V. Parasyuk, O.Y. Khyzhun, Opt. Mater. 114 (2021) 110982.
[53] C. Ambrosch-Draxl, J.O. Sofo, Comput. Phys. Commun. 175 (1) (2006) 1–14.
[54] F. Wooten, Optical Properties of Solids, Academic Press, New York, 1972.